



ORIGINAL ARTICLE

The role of citrate in heterogeneous silver metal catalyst formation: A mechanistic consideration



Christian Biermaier, Carolin Gleißner, Thomas Bechtold, Tung Pham *

Research Institute of Textile Chemistry and Textile Physics, University of Innsbruck, Austria, Hoehsterstrasse 73, 6850 Dornbirn, Austria

Received 14 November 2022; accepted 9 March 2023
Available online 16 March 2023

KEYWORDS

Silver catalyst;
Tollens' reaction;
Electroless copper deposition;
Heterogeneous catalyst formation;
Kolbe electrolysis

Abstract The formation of silver particles as initial catalyst for the electroless copper deposition is an essential part of the formation of conductive structures in flexible electronics. In this work, we have investigated the basic mechanism using the citrate anion for the fixation of silver species and later metal catalyst formation directly on a textile substrates surface. During the particle formation process and the subsequent electroless copper deposition, silver changes its oxidation state several times. While the decomposition of bulk silver citrate leads to silver metal, the distribution on the substrate surface leads to silver oxide due to the oxidation under air. Finally, the reducing conditions in the copper deposition step, i.e. alkaline formaldehyde, convert any silver-ion to silver metal. In parallel, the thermal decomposition of silver citrate also forms CO₂ and hexane-2,5-dione. The latter is the result of an auto oxidation reaction similar to *Kolbe electrolysis*, i.e. symmetrical radical recombination of two acetyl radicals remaining from the decarboxylated citrate scaffold.

© 2023 The Author(s). Published by Elsevier B.V. on behalf of King Saud University. This is an open access article under the CC BY license (<http://creativecommons.org/licenses/by/4.0/>).

1. Introduction

Flexible electronic textiles have become an integrated part in daily life with numerous applications in sports, safety, healthcare, etc. and attracted increased attention of the scientific community over the last decades. One major aspect of electronic textiles is the integration of conductive materials into isolating conventional textile substrates to connect the different assembled parts. A late trend within this field of interest is the generation of conductive lines by utilising decompos-

able self-reducing metal salts (metal precursors) for printing techniques (Yang et al., 2019). Copper inks contain mainly copper(II)-formate and need special protecting ligands to avoid oxidation by air (Dong et al., 2018; Xu & Wang, 2017; Yabuki et al., 2014). The topic is dominated by silver inks using thermally decomposable silver carboxylates (Nie et al., 2012; Yang et al., 2018). An example can be silver formate in an acrylate matrix (Krawczyk et al., 2021). After thermal decomposition, a conductive metal film remains from the printed lines due to reduction of silver(I) during decarboxylation. A parallel emerging trend is the utilisation of electroless copper deposition (ECD) (Ali et al., 2020; Chen et al., 2016; Landsiedel et al., 2020; Root et al., 2018; Wang et al., 2016) for the generation of conductivity on flexible substrates. Most common is the reduction of dissolved copper(II)-complexes in alkaline solution with formaldehyde. The ECD reaction is catalysed by metal surfaces and thus needs an initial metal catalyst (Ghosh, 2019). As an example, palladium(II)-chloride was used to form Pd seeds (Liu et al., 2010). Also, silver(I) salts can be reduced

* Corresponding author.

E-mail address: Tung.Pham@uibk.ac.at (T. Pham).

Peer review under responsibility of King Saud University.



by tin(II)-chloride (Root et al., 2018) and glucose (Wang et al., 2013) for the generation of silver metal as initial catalyst. Alternatively, silver (I) can also be reduced by thermal decomposition of a silver carboxylate as mentioned above. Chen *et al.* printed a silver citrate ink onto polyimide sheets and performed subsequent ECD for gaining electrical conductivity (Chen et al., 2016). In our former works, silver citrate has been precipitated directly on textile substrates by immersion of a citrate impregnated fabric into a silver nitrate solution (Gleissner et al., 2022) or by printing of a silver nitrate solution onto a citrate impregnated fabric (Biermaier et al., 2022). The conductive percolation was established by ECD. Especially the localised electroless copper deposition demonstrated the necessity of silver for initiation, as unprinted areas remained unplated. Also, an increase of the silver content led to a faster establishment of percolation by moving the percolation establishment zone towards lower deposition durations. Detailed description of the experimental procedures can also be found within the specimen manufacturing for the investigation of the functional ageing of copper plated fabrics (Biermaier et al., 2023).

The use of silver citrate as precursor for the formation of metal is based on the reductive decarboxylation of organic carboxylates. There are several decomposition mechanisms discussed in literature. They depend on the organic carboxylates and the reaction conditions of the decomposition. In a study by Roge *et al.*, the decomposition of silver(I)-ethylenediaminetetraacetic acid (EDTA) salts with different mol ratios of silver(I) content per EDTA, were investigated. A development of 0.5 mol CO₂ per mol silver metal was found for low silver(I) content. This led to the conclusion that two electrons were transferred to two silver(I)-ions during the elimination of a single CO₂ molecule. For silver(I) rich EDTA salts, one mol CO₂ was developed per mol silver-metal (Roge et al., 2000). So, only one electron was transferred from the carboxylate to the silver(I)-ion. The result agrees with the mechanism proposed by Fields *et al.* (Fields & Meyerson, 1976). It describes the homolytic cleavage of the Ag-O bond as initial step of silver carboxylate decomposition. A silver atom and a carboxylic radical are formed. The latter eliminates CO₂ and an organic radical remains (Fig. 1). Subsequently, further radical reactions and corresponding organic products are possible (Fields & Meyerson, 1976).

Burleva *et al.* reported that the thermal decomposition of silver succinate (C4-scaffold) results in metallic silver, CO₂ and ethylene (C2-scaffold) (Burleva et al., 1988). Hence, the remaining di-radicals after CO₂ elimination recombined. For silver oxalate, the authors found that the C-C-bond between the carboxylates is weakened and thus breaks first before transferring an electron to each silver(I) (Burleva et al., 1988). Other research also suggested, that silver carboxylates dissociate and form a carboxylic acid anhydride and silver(I)-oxide as an intermediate step (Szczęsny & Szyk, 2013). A different decomposition mechanism is suggested for aqueous solutions of silver-ions with an excess of deprotonated citrate. In an initial reaction step, the citrate decomposes by eliminating one CO₂ molecule, along with the formation of 3-ketoglutarate. Two electrons are transferred to reduce two silver(I)-ions. The silver atoms then form silver particles. Further decomposition of the citrate anion and reduction of silver(I) takes place on the surface of the silver particles acting as a catalyst (Patra et al., 2014). Although a number of publications exists, there is no clear description of the thermal decomposition mechanism that can be applied to all silver(I)-carboxylate derivatives. There is a strong dependence from the organic rest of the carboxylate and the surrounding conditions (Uvarov et al., 1998). Additionally, some mechanisms, as for the decomposition of silver citrate, are still not fully understood.

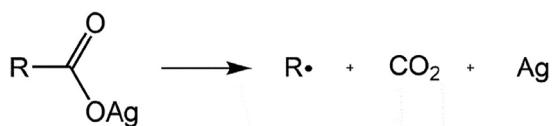


Fig. 1 Decomposition of a silver carboxylate.

In this work, we have investigated the role of solid silver citrate as a precursor for the heterogeneous silver metal catalyst formation on textile substrates. As a result, we are able to propose a mechanism for the description of the thermal decomposition process of solid silver citrate and clarify the different oxidation states of the silver on a textile substrate during the catalyst formation and subsequent electroless copper deposition process and in the different manufacturing stages from our previous work (Biermaier et al., 2022, 2023; Gleissner et al., 2022).

2. Experimental

2.1. Materials

Silver nitrate (AgNO₃, 99.9% p.a.) was purchased from Carl Roth GmbH und Co. KG, Karlsruhe, Germany. Trisodium citrate dihydrate (C₆H₅Na₃O₇·2H₂O, p.a.) was purchased from Merck KGaA, Darmstadt, Germany. Nitric acid (HNO₃ 65%, p.a.) was purchased from Chemlab NV, Zedelgem, Belgium. Ethanol (C₂H₆O 99.8%, denaturated) was purchased from Carl Roth GmbH und Co. KG, Karlsruhe, Germany. Ammonia (NH₃, 25%, p.a.) was purchased from Carl Roth GmbH und Co. KG, Karlsruhe, Germany. Hexane-2,5-dione (C₆H₁₀O₂, 97%) was purchased from Fisher Scientific GmbH, Schwerte, Germany. Silver(I) oxide (Ag₂O, 99%), silver(I) carbonate (Ag₂CO₃, 99%) and silver(I) acetate (AgC₂H₃O₂, 99.99%) were purchased from Merck KGaA, Darmstadt, Germany. Plain woven cellulose fabric (Lyocell) with a mass per unit area of 127 g/m² and yarn density of 39 warp/cm and 30 weft/cm, staple yarn, was kindly provided by Lenzing AG (Lenzing, Austria). The fabrics were LASER-cut to a sample size of 22 cm (warp direction) and 2.5 cm (weft direction).

2.2. Sample preparation

2.2.1. Citrate impregnation

The regenerated cellulose (Lyocell) fabric specimen strips were immersed in 100 mL 26 mM aqueous trisodium citrate dihydrate solution for 10 s each and subsequently padded at 3 bar pressurised air and a speed of 1 m/min using the padder Mathis HVF 33593 (Werner Mathis AG, Oberhasli, Switzerland). A water uptake of 79 ± 2% was found under these conditions. The specimens were subsequently dried in an air-ventilation oven for 5 min at 120 °C and 2300 rpm.

2.2.2. Silver-precursor formation on fabrics

The citrate-impregnated specimens were immersed into 100 mL 29 mM aqueous silver nitrate solution for 10 s and subsequently rinsed with 40 mL deionised water. The specimens were dried at ambient conditions.

2.2.3. Silver ion extraction

After different treatment of the silver citrate containing specimens S1-S6 as described below, three probes, each 50 mg, were drawn from each specimen and extracted for 4 min with 8 mL 5% ammonia. The extraction solutions were transferred into 100 mL volumetric flasks. 6 mL of HNO₃ 65% were added and filled to 100 mL. The solutions were investigated by means of F-AAS.

2.2.4. Silver citrate preparation

0.58 g trisodium citrate dihydrate were dissolved in 20 mL deionised water. 1.0 g silver nitrate were dissolved in 20 mL

water. The citrate-solution was added to the stirred silver-ion solution within 3 min and stirred for 20 min. After vacuum filtration, the colourless precipitate was washed five times with 20 mL deionised water and four times with 20 mL ethanol. To avoid heating, the precipitate was pre-dried under a permanent vacuum-induced air-stream for 1 h.

2.2.5. Preparation of decomposition product

Freshly prepared silver citrate was pre-dried at 105 °C in air for 45 min. 0.75 g of the obtained product were heated in a 250 mL round bottom flask until occurrence of the quick and strong exothermal reaction. A cooling finger was inserted that contained water at ambient temperature in order to avoid condensation of moisture from air. The collected product was extracted with ethanol. The ethanol was removed by a rotation evaporator.

2.3. Analytics

2.3.1. Silver content determination

The silver content was determined using an F-AAS contra 300 device from Analytik Jena (Jena, Germany) in nitric acidic milieu (3% HNO₃) at 338 nm with an acetylene/air-flame in a 100 mm burner. The calibration was done by linear regression (Supporting information – Fig. S1).

2.3.2. Thermal analysis

The investigation of the thermal decomposition was performed using the TGA 2 - Star e System and a DSC 3 - Star e System from Mettler Toledo (Columbus, US). Beside standard heating rate of 10 K/min, a slower heating rate of 1 K/min was also applied for a detailed resolution including a pre-drying phase at 10 K/min. The slow TGA was performed with low amounts of sample substance of ca. 0.9–1.4 mg.

2.3.3. Infrared spectroscopy

The attenuated total reflectance (ATR) of the formed products was recorded in the spectra range of 4000 to 600 cm⁻¹ using the FTIR spectrometer Invenio S (Bruker Optik GmbH Ettlingen, Germany) with a resolution of 2 cm⁻¹ and 64 scans per measurement.

2.3.4. Scanning Electron Microscopy (SEM) and Energy Dispersive X-Ray Spectroscopy (EDX)

Scanning electron images were taken using the benchtop Hitachi TM 3030 (Hitachi, Ltd., Tokyo, Japan) at a voltage of 15 kV. The samples were coated with 25 nm gold by physical vapour deposition. The EDX measurements were performed using the Bruker Quantax 70 detector.

3. Results and discussion

3.1. Investigation of the silver oxidation state

In a previous work (Gleissner et al., 2022), the functionality of citrate as surficial binder for silver(I)-ions was demonstrated. The surficial existence of a silver species after precipitation of silver citrate was proven by SEM imaging. It showed particles and flake-like structures on the fibre surface (Supporting Information – Fig. S2). In accompanying EDX measurements, silver

was found along a yarn (Supporting Information – Fig. S3 and S4). EDX mapping on a SEM image showed the equal distribution of silver on the Lyocell fabric surface (Supporting information – Fig. S5).

Throughout the manufacturing the colour of silver citrate impregnated specimen changed from colourless for the untreated fabric (Fig. 2a) to brown after thermal treatment at 160 °C (Fig. 2b) and further to black in alkaline solution of formaldehyde (reduction agent in ECD solution, Fig. 2c), becoming brownish while storage at air. These changes of colours are strong hints for surficial redox reactions.

Further investigation needed separation of metallic silver from silver(I) ions. In order to distinguish between both in the different steps of the reduction, ammonia solubility was used to extract silver(I)-ions in a silver diamine complex. A 5% ammonia solution was used for the extraction of differently treated specimen (Table 1). The extraction solution was then acidified to a concentration of 5% HNO₃ for further analysis by F-AAS. Resulting high silver values in the extraction solution indicated a good solubility of the impregnation and thus, the occurrence of silver(I). Resulting low silver values in the extraction solution indicated an insoluble silver species, i.e., metallic silver adsorbed to the textile surface. The treatment conditions and results are listed in Table 1.

Specimen S1 is the untreated sample after silver citrate formation on the surface of the fabric, which was extracted by ammonia solution and by 30% nitric acid, respectively. The extractions are considered as full removal of all silver from the fabric. In both cases, the extracted silver content was about 3%. Specimen S2 was treated with 0.25 M NaOH before the ammonia extraction, which is the approximate alkali content of an ECD solution (Root et al., 2018). The extracted silver content in S2 (brownish) was 2.2% which is considered as silver(I). The difference to S1 could be explained by the loss of silver(I) during the treatment with NaOH (Arata, 1998; Johnston et al., 1933). Specimens S3-S5 were immersed into an alkaline formaldehyde solution with equal concentration as in an ECD solution, i.e. the electroless copper deposition solution was simulated but without copper ions (Root et al., 2018). The values of extracted silver strongly decreased to 0.45–0.84%. This observation can be explained by the reduction of silver(I) to non-extractable silver metal adhering to the substrate surface. The reduction reaction is also known from the Tollens' probe for aldehydes for distinguishing reducing sugars in ancient analytics (silver mirror probe) (Tollens, 1882). The reaction is also known from the generation of silver nanoparticles (Chou & Ren, 2000) or in formaldehyde sensors (Chaiendoo et al., 2018). After 3 min of reaction (S3), the extractable silver content was 0.84%, which was far below the value of sample S2 (treated with NaOH only). After 15 min (S4) and 30 min (S5) reaction, the extractable silver content went further down to 0.45–0.56%. The strong decreases of extractable silver(I) content clearly proved that the formation of metallic silver in the presence of formaldehyde and led to the conclusion that the reduction from silver (I) to metallic silver takes place directly before the start of the copper deposition during the subsequent ECD step.

An extractable silver content of 2.68% was found for specimen S6, which was heated to 160 °C to decompose silver citrate. As insoluble silver metal was expected as result of the thermal silver carboxylate decomposition, we assumed that a silver(I)-species, supposedly silver(I)-oxide, was formed on

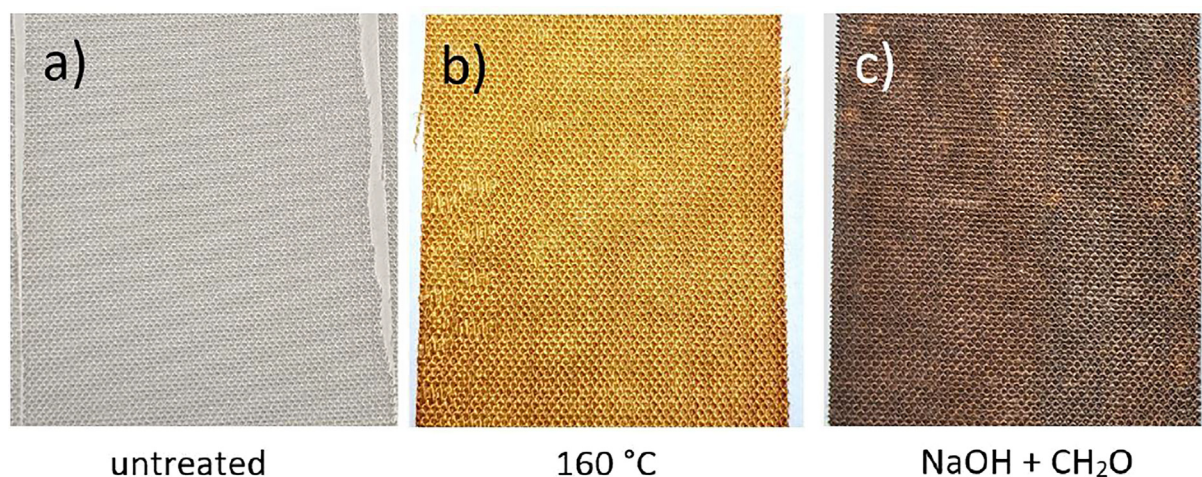


Fig. 2 Visual appearance of silver citrate containing Lyocell fabrics at different stages of manufacturing, a) untreated, b) after thermal decomposition at 160 °C in an air ventilation oven and c) after immersion into alkaline formaldehyde with some time elapsed due to drying at ambient conditions.

Table 1 Extractable silver content from silver citrate impregnated Lyocell specimens with different treatment conditions.

Specimen	Treatment after silver citrate formation on fabric	Mass percent silver extracted from specimen (%)
S1	dried at ambient conditions in air, HNO ₃ extract	3.61 ± 0.60
S1	dried at ambient conditions in air, NH ₃ extract	3.04 ± 0.14
S2	100 mL 0.25 M NaOH, 35 min	2.19 ± 0.18
S3	100 mL of 0.25 M NaOH + 0.35 M CH ₂ O, 3 min	0.84 ± 0.04
S4	100 mL of 0.25 M NaOH + 0.35 M CH ₂ O, 15 min	0.45 ± 0.04
S5	100 mL of 0.25 M NaOH + 0.35 M CH ₂ O, 30 min	0.56 ± 0.07
S6	160 °C and 2300 rpm air vent., 10 min	2.68 ± 0.03

the textile surface as a result of oxidation by air after the thermal decomposition.

3.2. Investigation of silver citrate decomposition

The thermal behaviour of solid silver citrate has been investigated via differential scanning calorimetry (DSC) and thermogravimetry (TGA) by Nie and Yang (Nie et al., 2012; Yang et al., 2018). Their DSC result proved a strong exothermy of the decomposition reaction with a maximum peak between 190 °C and 198 °C. The authors also report that the TGA curves showed a strong step-like weight loss during reaction of about 36% to 40% of the original sample in the same temperature range as DSC. These findings are supported by our own measurements (Supporting information – Fig. S6).

As the reaction occurs very fast after reaching the temperature of about 190 °C and the resolution of DSC curves is not sufficient to provide more information on the different stages of the decomposition, we decided to utilise TGA with a much lower heating rate of 1 K/min (instead of 10 K/min, as done in the literature above) to resolve better weight loss as function of the reaction temperature. The attempt was done to provide more time for different reaction stages or intermediates before the full decomposition. The results of the relevant temperature range from 140 °C to 220 °C of such slow TGA investigation are shown in Fig. 3. The final weight loss of the sample under nitrogen atmosphere was found as 37.4% of

the original mass. The value is in the range of the theoretical value of the citrate molecule (36.9% as calculated in Table 2). This clearly indicated the full decomposition of the citrate molecules, yielding silver metal as solid bright greyish residue. For an additional evaluation, the mathematical first derivation was applied to estimate the slope of the weight loss. It showed a dominant negative double peak (Fig. 3), indicating a short period of decreased rate of weight loss, despite continuously increasing temperature. This observation could be interpreted as the formation of a metastable intermediate with a decomposition temperature close to silver citrate. The inter-peak negative minimum was located at 162.8 °C with the corresponding weight loss of 18.7%. In comparison to Table 2, the value indicated the elimination of 2 CO₂ (equal to 17.2%). The difference between the measured and theoretical value can be attributed to two effects. At first, the high slope of the weight loss in this area provided room for inaccuracy. Secondly, the double peak did not show baseline separation. Assuming Gaussian distribution of each single peak, the overlap takes place in favour of the higher peak and thus, the total value is increased.

The educts and products were further investigated using infrared spectroscopy. The IR spectrum of silver citrate (Fig. 4, curve a) shows characteristic bands at 3224 cm⁻¹ (ν OH), 2960 cm⁻¹ (ν CH), 1538 cm⁻¹ (ν C=O), 1402 cm⁻¹ (δ CH), 1291 cm⁻¹ (ν C–O), 1137 cm⁻¹ (ν C–O) which is in accordance to the results shown by Yang et al. (Yang et al.,

2018). The silver citrate probe was heated at air to 155 °C for a few minutes and the IR-absorption was measured again, (Fig. 4, curve b) which showed shrinking bands, but no newly occurring ones. The full decomposition in air (Fig. 4, curve c) and under N₂-atmosphere (Fig. 4, curve d) did not show any molecule signals at all. Hence, there were no organic molecules leftover, i.e. the decomposition released only volatile products except silver metal. This is well in line with the results of the TGA. Also, the bulk formation of silver carbonate and oxide can be excluded by the IR spectra (Slager et al., 1972). The TGA of commercial silver carbonate also excludes the formation of silver carbonate after silver citrate decomposition, as it decomposed at about 150 °C to form silver oxide being stable until about 350 °C (Supporting Information – Fig. S7). The bright greyish colour and a metallic gloss of the solid decomposition product after pressing onto the ATR-crystal of the IR device supported the fact that metallic silver was formed in samples heated in air and N₂-atmosphere. These findings are well in line with the observation reported in the literature where the thermal decomposition of silver carboxylates results in silver metal formation (Lim et al., 2020; Yang et al., 2018).

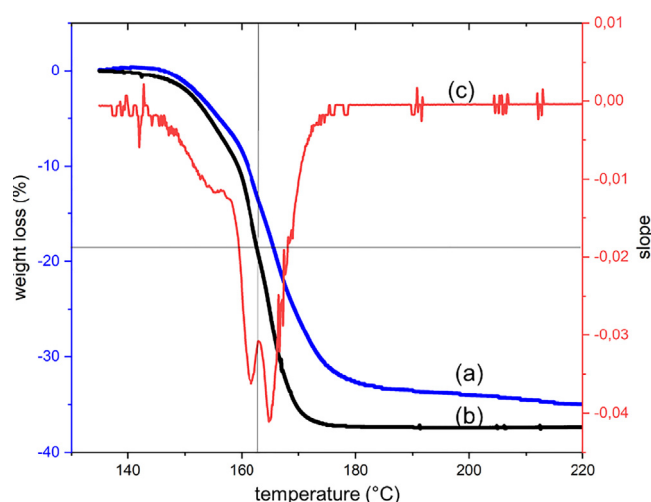


Fig. 3 TGA curves with 1 K/min heating rate of (a) silver citrate in air, (b) silver citrate in N₂ and (c) first derivation of the curve b.

Table 2 Theoretical mass percent of selected atoms and molecules in silver citrate.

Compound	M (g/mol)	Content in silver citrate in %
H ₂ O	18.02	3.5
CO ₂	44.01	8.6
2CO ₂	88.02	17.2
3 CO ₂	132.03	25.8
Citrate C ₆ H ₅ O ₃ ³⁻	189.13	36.9
Ag	107.87	21.0
3Ag	323.61	63.1
3/2 Ag ₂ O	347.61	67.8
Ag ₃ C ₆ H ₅ O ₇	512.70	100

The combination of TGA and IR measurements proved the full elimination of the organic part of silver citrate by heating up to 200 °C. For further investigation of the volatile organic part, decomposition products of the reaction were collected using the experimental setup shown in Fig. 5. For this purpose, a cooling finger was placed above the decomposition reaction. To avoid the interference of water, the freshly prepared silver citrate was dried at 105 °C for 45 min in advance. The setup was heated and the sample became dark at the edges before reaction occurred. Immediately after the fierce and fast decomposition reaction, a brownish oily substance condensed on the cooling finger along with the formation of mist.

Besides, a grey solid substance remained at the place of the sample substance after the reaction. The cooling finger and the flask were rinsed with ethanol. The solution was filtered and the solvent was removed by a rotary evaporator. The obtained brownish oil was collected with a pipette tip and transferred to an ATR-crystal for IR spectroscopy. Fig. 6 shows the IR spectrum of the collected organic decomposition product after extraction (b) compared to the spectrum of hexane-2,5-dione (a). A flat broad peak at 3200 cm⁻¹ and the shoulder at 1600 cm⁻¹ are assumedly due to water residues. Characteristic peaks located at 2922, 2850, 1708, 1405, 1362, 1226, 1163 cm⁻¹ fit very well to the spectrum of purchased hexane-2,5-dione (a) as well as to the result published by NIST/Coblentz Society for hexane-2,5-dione vapour (Zeller, 1977). The brownish colour is possibly due to silver/silver oxide traces that were emitted in the quick exothermal reaction, together with hexan-2,5-dione.

Nonetheless, a possible error source was the open flask that left the possibility of easy volatile products, especially CO₂, to escape. Also, the extraction with ethanol and its distillative removal could have removed further volatile by-products.

3.3. Mechanistic consideration of silver citrate decomposition

The presented results demonstrated the elimination of two CO₂ molecules as the initial step and the formation of hexane-2,5-dione as the final step during the thermal decomposition of silver citrate to form silver metal catalyst. For the explanation of the reaction pathway, we propose the following

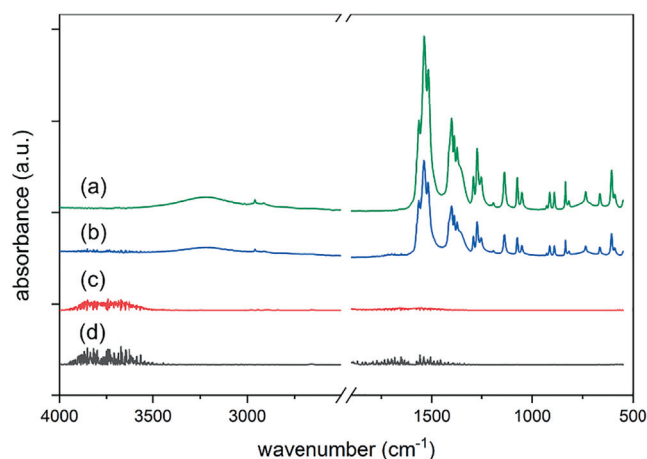


Fig. 4 IR-spectra of silver citrate after (a) drying at 105 °C, (b) heating to 155 °C, (c) heating to 200 °C in air and (d) heating to 200 °C in N₂.

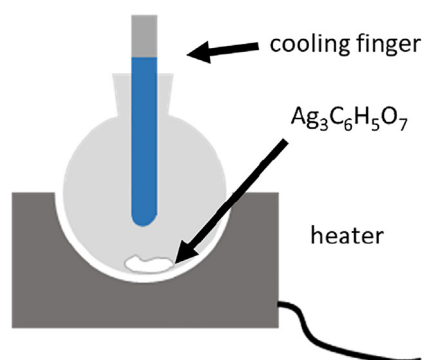


Fig. 5 Experimental setup to collect decomposition products of the reaction with a cooling finger at ambient temperature (*CAUTION: The strong exothermic reaction and the gas expansion allowed only a small amount of dried silver citrate is allowed to be decomposed in a big flask for preparative reasons, here 0.75 g in 250 mL, operation in fume hood and in safety cage*).

thermal decomposition sequences of solid silver citrate. For the sake of simplicity, we resort to a single silver citrate molecule and consider its embedment into a crystal structure (Fischer, 2011).

As shown in Fig. 7, the full thermal decomposition of silver citrate consists of 4 steps. Initially in step I, the carboxylate attached to C3 in silver citrate (a), is eliminated as CO_2 by an electron pair mechanism. This includes the distribution of two electrons to two silver(I), assumedly by two single electron transfers (SETs). This part of the mechanism has been suggested for diluted solutions with an excess of citrate by Patra, Lim and Ojea-Jiménez (Lim et al., 2020; Ojea-Jiménez & Campanera, 2012; Patra et al., 2014). The proton of the hydroxyl group at C3 is accepted by the free carboxylic group that does not contain a silver(I)-ion anymore. This is supported by the crystal structure of silver citrate presented by Fischer (Fischer, 2011). It identifies an H-bond between the hydroxyl group and one oxygen of the carboxylic group. Hence, a six membered structure is formed, in which the proton can be

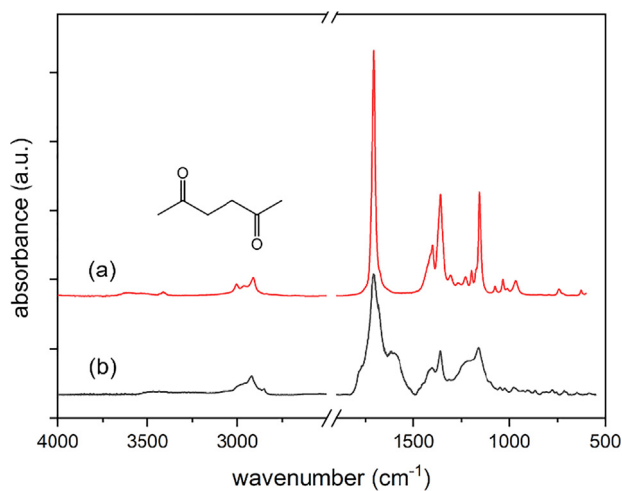


Fig. 6 IR spectra of purchased hexane-2,5-dione (a) and collected decomposition product (b).

transferred. A 3-ketoglutarate silver salt (b) remains from the citrate scaffold. As β -keto carboxylates are very labile compounds, decarboxylation is initiated with a six membered ring intermediate structure as before (Ignatchenko et al., 2017; Logue et al., 1975; Pedersen, 1929) (step II). The subsequent decarboxylation forms an enol that rearranges due to keto-enol tautomerism (Bigley & Thurman, 1968; Fischer, 2011; Lim et al., 2020; Zeller, 1977). The symmetry of the 3-ketoglutarate (b) provides two carboxylic groups neighbored to the ketone. The carboxylic acid decomposes favoured and faster than the carboxylic anion (Guthrie, 2002; Hay & Bond, 1967). The silver(I) containing carboxylate persists during decarboxylation. In this decarboxylation step, no silver is reduced and the oxo-butanoic silver salt (c) is formed. This is again a β -keto carboxylate. However, there is no proton involved to form a six-membered transition state. It can be assumed that further decomposition starts with a homolytic Ag-O bond cleavage (step III) as described for other silver carboxylates (Fields & Meyerson, 1976). Subsequently, an elimination of a CO_2 -molecule leaves an acetylonyl radical (d).

The combination of step III and step IV shows a radical decarboxylation followed by a symmetrical radical recombination of two acetylonyl radicals and the formation of hexane-2,5-dione (e) as detected above by IR spectroscopy. Another example from literature for this combination of reactions is reported for silver benzoate (Fields & Meyerson, 1976). It decomposes to silver metal, CO_2 and further products, especially biphenyl. The reaction is similar to the Kolbe electrolysis, where the radical decomposition of carboxylates via CO_2 elimination is initiated by the application of an electrical current at the anode (Kolbe, 1849). In our case, silver(I) works as an internal anode and the reaction is likely a Kolbe auto-oxidation. An example of the application of silver carboxylate radical generation for an unsymmetrical radical reaction is summarised in a work of Studer (Studer, 2012). Silver trifluoroacetate is used to generate the trifluoromethyl radical by heat or radiation (Fields & Meyerson, 1976; Studer, 2012).

Another analogy for the decomposition mechanism of silver citrate is the decomposition of citric acid under concentrated sulphuric acid condition. In a first step, the carboxylic group attached to C3 is eliminated as CO and water with leaving acetonedicarboxylic acid. The latter decomposes to 2 CO_2 and acetone (Wiig, 1930). In this case, the carbon atom in CO with the oxidation state + II keeps two electrons that were distributed to two Ag^+ for silver citrate under the elimination of CO_2 with the oxidation state + IV for the carbon atom. The acetone also keeps an electron in comparison to the acetylonyl radical. This excess electron was transferred to the last Ag^+ for silver citrate. However, in a work on the thermal decomposition of citric acid, Wyrzykowski *et al.* determined two intramolecular dehydrations as a first and a second step. *Trans*-aconitic acid and its anhydride are formed. A following decarboxylation then formed either citraconic anhydride or itaconic anhydride. They were both found in the volatile decomposition products (Wyrzykowski et al., 2011). Similar decomposition products were found for salts of citrate with non-oxidising counter-ions like calcium or barium (Srivastava et al., 1984). Hence, the oxidising character of the silver(I)-ion is clearly responsible for initiating the first decarboxylation step shown in Fig. 7 (step I). Likely, the silver(I)-ion shifts the activation energy for the decarboxylation below the activation energy for a dehydration reaction

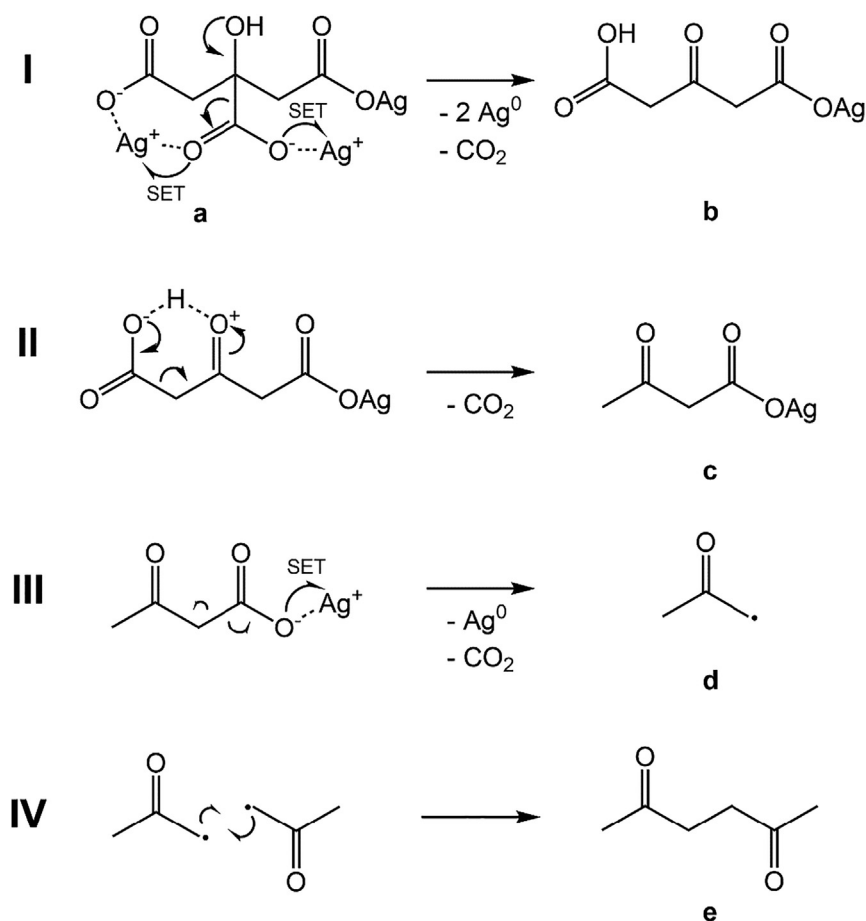


Fig. 7 Proposed mechanism of the thermal silver citrate decomposition.

among the citrate scaffold as occurring for pure citric acid and its calcium or barium salts.

We consider the presented mechanism as plausible. However, for a detailed analysis of the mechanism, the crystal structure of the solid substance needed to be fully included, as well as the half-lifetime and crystal structures of possible intermediates. Especially the structure of the β -keto-carboxylate seems to play a role for its decomposition rate (Hatamura et al., 2015). This however is difficult to estimate, as the intermediate product is assumedly impurified by silver metal particles and it decomposes directly after its synthesis, i.e. its structure may be influenced by the structure of the silver citrate.

4. Conclusions

The present investigations addressed the mechanism of the thermal decomposition of silver citrate and the metamorphosis of silver during the subsequent electroless copper deposition. After the precipitation of silver citrate, the thermal decomposition of the pure silver citrate led to silver metal. The thermal decomposition of silver citrate distributed on textile substrates led to the formation of silver(I). The simulation of an electroless copper deposition process with an alkaline formaldehyde solution led to the formation of ammonia insoluble silver metal. The formed silver metal particles and islands then would be able to act as initial catalyst that is necessary for starting the reduction of cop-

per(II) in the ECD process, forming desired conductive lines on the flexible textile substrates. From the citrate perspective, the thermal decomposition of silver citrate led to the elimination of two CO_2 molecules in short succession. This can be explained by a first reductive decarboxylation of the carboxylic acid attached to C3, wherein two silver ions are reduced. The lability of the ketoglutarate silver salt led to an immediate non-reductive second decarboxylation of the free carbon acid. The oxo-butanoic silver salt was supposedly a short-lived *meta*-stable intermediate that was indicated by thermogravimetry. A final reductive decarboxylation left an acetyl radical from the citrate scaffold that formed hexane-2,5-dione by symmetrical recombination.

The investigations showed that the role of the citrate in silver metal catalyst formation in a fine distribution is not from a reductive nature, as basically no pre-reduction of silver(I) on a fabric surface before immersing into an ECD solution is necessary for starting ECD. However, citrate is able to precipitate silver on a fabric surface.

CRedit authorship contribution statement

Christian Biermaier: Conceptualization, Methodology, Investigation, Writing – original draft, Visualization. **Carolin Gleißner:** Methodology, Investigation, Writing – review & editing. **Thomas Bechtold:** Conceptualization, Methodology, Writing – review & editing. **Tung Pham:** Conceptualization, Resources, Writing – review & editing, Supervision, Funding acquisition.

Declaration of Competing Interest

The authors declare that they have no known competing financial interests or personal relationships that could have appeared to influence the work reported in this paper.

Acknowledgment

Financial support is gratefully acknowledged to the project “SmartTexAging – FFG 874746” funded by the Austrian Research Promotion Agency FFG and the COMET project “Textile Competence Center Vorarlberg 2 – FFG 882502” funded within COMET – Competence Centers for Excellent Technologies – by BMK, BMDW as well as co-financing federal province Vorarlberg. The COMET-Funding Program is managed by the Austrian Research Promotion Agency FFG.

Appendix A. Supplementary material

Supplementary data to this article can be found online at <https://doi.org/10.1016/j.arabjc.2023.104803>.

References

- Ali, A., Baheti, V., Vik, M., Militky, J., 2020. Copper electroless plating of cotton fabrics after surface activation with deposition of silver and copper nanoparticles. *J. Phys. Chem. Solid* 137. <https://doi.org/10.1016/j.jpcs.2019.109181>.
- Arata, A.B., 1998. US6197814B1.
- Biermaier, C., Gleißner, C., Bechtold, T., Pham, T., 2022. Localised catalytic printing for flexible conductive lines by electroless copper deposition on textiles. *IEEE Int. Conf. Flexible Printable Sensors Syst. (FLEPS)*. <https://doi.org/10.1109/FLEPS53764.2022.9781518>.
- Biermaier, C., Petz, P., Bechtold, T., Pham, T., 2023. Investigation of the functional ageing of conductive coated fabrics under simulated washing conditions. *Materials* 16 (3), 912. <https://doi.org/10.3390/ma16030912>.
- Bigley, D.B., Thurman, J.C., 1968. *Studies in Decarboxylation. Part VI.1 A Comparison of the Transition States for the Decarboxylation of P-Keto- and py-Unsaturated Acids*. *J. Chem. Soc. B*, 436–440.
- Burleva, L., Andreev, V., Boldyrev, V., 1988. Thermal decompositions of silver carboxylates. *J. Therm. Anal.* 33, 735–739.
- Chaiendoo, K., Sooksin, S., Kulchat, S., Promarak, V., Tuntulani, T., Ngeontae, W., 2018. A new formaldehyde sensor from silver nanoclusters modified Tollens’ reagent. *Food Chem.* 255, 41–48. <https://doi.org/10.1016/j.foodchem.2018.02.030>.
- Chen, J.J., Zhang, J., Wang, Y., Guo, Y.L., Feng, Z.S., 2016. A particle-free silver precursor ink useful for inkjet printing to fabricate highly conductive patterns. *J. Mater. Chem. C* 4 (44), 10494–10499. <https://doi.org/10.1039/c6tc03719d>.
- Chou, K.-S., Ren, C.-Y., 2000. Synthesis of nanosized silver particles by chemical reduction method. *Mater. Chem. Phys.* 64.
- Dong, Y., Lin, Z., Li, X., Zhu, Q., Li, J.G., Sun, X., 2018. A low temperature and air-sinterable copper-diamine complex-based metal organic decomposition ink for printed electronics. *J. Mater. Chem. C* 6 (24), 6406–6415. <https://doi.org/10.1039/c8tc01849a>.
- Fields, E.K., Meyerson, S., 1976. Thermal and photochemical decomposition of silver carboxylates. *J. Org. Chem.* 41 (6), 128.
- Fischer, A., 2011. Trisilver(I) citrate. *Crystallogr. Commun.* 67, (2) m255.
- Ghosh, S., 2019. Electroless copper deposition: A critical review. In: *Thin Solid Films*, 669. Elsevier B.V, pp. 641–658. <https://doi.org/10.1016/j.tsf.2018.11.016>.
- Gleißner, C., Biermaier, C., Bechtold, T., Pham, T., 2022. Complexation-mediated surface modification of polyamide-66 textile to enhance electroless copper deposition. *Mater. Chem. Phys.* 288. <https://doi.org/10.1016/j.matchemphys.2022.126383>.
- Guthrie, J.P., 2002. Uncatalyzed and amine catalyzed decarboxylation of acetoacetic acid: An examination in terms of No Barrier Theory. *Bioorg. Chem.* 30 (1), 32–52. <https://doi.org/10.1006/bioo.2001.1231>.
- Hatamura, M., Yamaguchi, S., Takane, S.Y., Chen, Y., Suganuma, K., 2015. Decarboxylation and simultaneous reduction of silver(I) β -ketocarboxylates with three types of coordinations. *Dalton Trans.* 44 (19), 8993–9003. <https://doi.org/10.1039/c5dt00773a>.
- Hay, R.W., Bond, M.A., 1967. Kinetics of the Decarboxylation of Acetoacetic acid. *Aust. J. Chem.* 20 (9), 1823–1828.
- Ignatchenko, A., McSally, J.P., Bishop, M.D., Zweigle, J., 2017. Ab initio study of the mechanism of carboxylic acids cross-ketonization on monoclinic zirconia via condensation to beta-keto acids followed by decarboxylation. *Mol. Catal.* 441, 35–62. <https://doi.org/10.1016/j.mcat.2017.07.019>.
- Johnston, H.L., Cuta, F., Garrett, A.B., 1933. The amphoteric character of silver hydroxide. *J. Am. Soc.* 55 (6), 2311–2325. <https://pubs.acs.org/sharingguidelines>.
- Kolbe, H., 1849. *Untersuchungen über die Elektrolyse organischer Verbindungen*. *Annalen Der Chemie Und Pharmacie* 69, 257–294.
- Krawczyk, K.K., Groten, J., Glushko, O., Krivec, M., Frühwirth, M., Schulz, G., Wolf, C., Hartmann, D., Moser, M., Cordill, M.J., Stadlober, B., Griesser, T., 2021. Self-Reducing silver ink on polyurethane elastomers for the manufacture of thin and highly stretchable electrical circuits. *Chem. Mater.* 33 (8). <https://doi.org/10.1021/acs.chemmater.0c04025>.
- Landsiedel, J., Root, W., Schramm, C., Menzel, A., Witzleben, S., Bechtold, T., Pham, T., 2020. Tunable colors and conductivity by electroless growth of Cu/Cu₂O particles on sol-gel modified cellulose. *Nano Res.* 13 (10), 2658–2664. <https://doi.org/10.1007/s12274-020-2907-5>.
- Lim, J.K., Liu, T., Jeong, J., Shin, H., Jang, H.J., Cho, S.P., Park, J.S., 2020. In situ syntheses of silver nanoparticles inside silver citrate nanorods via catalytic nanoconfinement effect. *Colloids Surf. A Physicochem. Eng. Asp.* 605. <https://doi.org/10.1016/j.colsurfa.2020.125343>.
- Liu, X., Chang, H., Li, Y., Huck, W.T.S., Zheng, Z., 2010. Polyelectrolyte-bridged metal/cotton hierarchical structures for highly durable conductive yarns. *ACS Appl. Mater. Interfaces* 2 (2), 529–535. <https://doi.org/10.1021/am900744n>.
- Logue, M.W., Pollack, R.M., Vitullo, V.P., 1975. The nature of the transition state for the decarboxylation of beta-keto acids. *J. Am. Chem. Soc.* 97 (23), 6868–6869. <https://pubs.acs.org/sharingguidelines>.
- Nie, X., Wang, H., Zou, J., 2012. Inkjet printing of silver citrate conductive ink on PET substrate. *Appl. Surf. Sci.* 261, 554–560. <https://doi.org/10.1016/j.apsusc.2012.08.054>.
- Ojea-Jiménez, I., Campanera, J.M., 2012. Molecular modeling of the reduction mechanism in the citrate-mediated synthesis of gold nanoparticles. *J. Phys. Chem. C* 116 (44), 23682–23691. <https://doi.org/10.1021/jp305830p>.
- Patra, S., Pandey, A.K., Sen, D., Ramagiri, S., Bellare, J.R., Mazumder, S., Goswami, A., 2014. Redox decomposition of silver citrate complex in nanoscale confinement: An unusual mechanism of formation and growth of silver nanoparticles. *Langmuir* 30 (9), 2460–2469. <https://doi.org/10.1021/la4048787>.
- Pedersen, K.J., 1929. The ketonic decomposition of beta-keto carboxylic acids. *J. Am. Chem. Soc.* 51 (11), 2098–2107. <https://pubs.acs.org/sharingguidelines>.

- Roge, A., Fiorucci, Â., Saran, L.M., der Tadeu, E.Â., Cavalheiro, G., Neves, E.A., 2000. Thermal stability and bonding in the silver complexes of ethylenediaminetetraacetic acid. *Thermochimica Acta* 356 (1–2), 71–78. [https://doi.org/10.1016/S0040-6031\(00\)00478-0](https://doi.org/10.1016/S0040-6031(00)00478-0).
- Root, W., Aguiló-Aguayo, N., Pham, T., Bechtold, T., 2018. Conductive layers through electroless deposition of copper on woven cellulose lyocell fabrics. *Surf. Coat. Technol.* 348, 13–21. <https://doi.org/10.1016/j.surfcoat.2018.05.033>.
- Slager, T., Lindgren, B.J., Mallmann, J., Greenler, R.G., 1972. The infrared spectra of the oxides and carbonates of silver. *J. Phys. Chem.* 76 (6), 940–943 <https://pubs.acs.org/sharingguidelines>.
- Srivastava, A., Singh, P., Gunjkar, V.G., Jose, C.I., 1984. Thermal decomposition of barium citrate. *Thermochim Acta* 76, 249–254.
- Studer, A., 2012. A “renaissance” in radical trifluoromethylation. *Angewandte Chemie – Int. Ed.* 51 (36), 8950–8958. <https://doi.org/10.1002/anie.201202624>.
- Szczęśny, R., Szyk, E., 2013. Thermal decomposition of some silver(I) carboxylates under nitrogen atmosphere. *J. Therm. Anal. Calorim.* 111 (2), 1325–1330. <https://doi.org/10.1007/s10973-012-2485-1>.
- Tollens, B., 1882. Ueber ammon-alkalische Silberlösung als Reagens auf Aldehyd. *Ber. Dtsch. Chem. Ges.* 15, 1635–1639.
- Uvarov, N.F., Burleva, L.P., Mizen, M.B., Whitcomb, D.R., Zou, C., 1998. Conductivity of long-chain silver carboxylates and their thermal decomposition products. In *Solid State Ionics* (Vol. 107).
- Wang, Y., Bian, C., Jing, X., 2013. Adhesion improvement of electroless copper plating on phenolic resin matrix composite through a tin-free sensitization process. *Appl. Surf. Sci.* 271, 303–310. <https://doi.org/10.1016/j.apsusc.2013.01.188>.
- Wang, Y., Wang, Y., Chen, J.J., Guo, H., Liang, K., Marcus, K., Peng, Q.L., Zhang, J., Feng, Z.S., 2016. A facile process combined with inkjet printing, surface modification and electroless deposition to fabricate adhesion-enhanced copper patterns on flexible polymer substrates for functional flexible electronics. *Electrochim. Acta* 218, 24–31. <https://doi.org/10.1016/j.electacta.2016.08.143>.
- Wiig, E.O., 1930. The decomposition of citric acid by sulfuric acid. *J. Am. Chem. Soc.* 52 (12), 4729–4737 <https://pubs.acs.org/sharingguidelines>.
- Wyrzykowski, D., Hebanowska, E., Nowak-Wicz, G., Makowski, M., Chmurzyński, L., 2011. Thermal behaviour of citric acid and isomeric aconitic acids. *J. Therm. Anal. Calorim.* 104 (2), 731–735. <https://doi.org/10.1007/s10973-010-1015-2>.
- Xu, W., Wang, T., 2017. Synergetic effect of blended alkylamines for copper complex ink to form conductive copper films. *Langmuir ACS J. Surf. Colloids* 33 (1), 82–90. <https://doi.org/10.1021/acs.langmuir.6b03668>.
- Yabuki, A., Tachibana, Y., Fathona, I.W., 2014. Synthesis of copper conductive film by low-temperature thermal decomposition of copper-aminediol complexes under an air atmosphere. *Mater. Chem. Phys.* 148 (1–2), 299–304. <https://doi.org/10.1016/j.matchemphys.2014.07.047>.
- Yang, W., List-Kratochvil, E. J. W., & Wang, C. (2019). Metal particle-free inks for printed flexible electronics. In: *J. Mater. Chem. C* (Vol. 7, Issue 48). Royal Society of Chemistry, pp. 15098–15117. <https://doi.org/10.1039/c9tc05463d>.
- Yang, W., Wang, C., Arrighi, V., 2018. An organic silver complex conductive ink using both decomposition and self-reduction mechanisms in film formation. *J. Mater. Sci. Mater. Electron.* 29 (4), 2771–2783. <https://doi.org/10.1007/s10854-017-8205-7>.
- Zeller, M., 1977. <https://webbook.nist.gov/cgi/cbook.cgi?ID=C110134&Units=SI&Type=IR-SPEC&Index=1#IR-SPEC>.